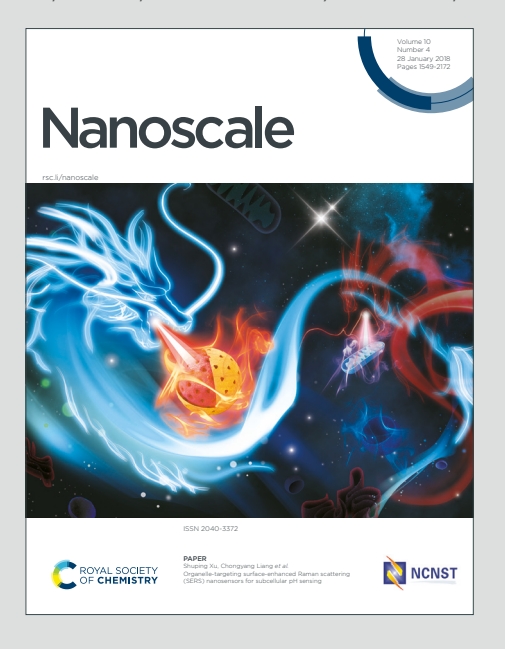




Nanoscale

Accepted Manuscript

This article can be cited before page numbers have been issued, to do this please use: F. Nie, H. Lin, X. Su, Q. Ren, X. Liu and K. Ou, *Nanoscale*, 2025, DOI: 10.1039/D5NR03427B.



This is an Accepted Manuscript, which has been through the Royal Society of Chemistry peer review process and has been accepted for publication.

Accepted Manuscripts are published online shortly after acceptance, before technical editing, formatting and proof reading. Using this free service, authors can make their results available to the community, in citable form, before we publish the edited article. We will replace this Accepted Manuscript with the edited and formatted Advance Article as soon as it is available.

You can find more information about Accepted Manuscripts in the <u>Information for Authors</u>.

Please note that technical editing may introduce minor changes to the text and/or graphics, which may alter content. The journal's standard <u>Terms & Conditions</u> and the <u>Ethical guidelines</u> still apply. In no event shall the Royal Society of Chemistry be held responsible for any errors or omissions in this Accepted Manuscript or any consequences arising from the use of any information it contains.



					VIEW ALTICLE OTHER
TT 1	1				DOI: 10•1039/D5NR03427B
Understa	anding intertac	ial interaction	characteristics	of asphalt	DOI: 10.1039/D5NR03427E

- 2 reinforced with diamond nanothread and carbon nanotube
- Fenghua NIE a, b, Hang LIN a, Xing SU a, Qifan REN a, Xuefeng LIU b, c, *, Ke OU d
- 4 a School of Resources and Safety Engineering, Central South University, Changsha,
- 5 China

- 6 b Department of Architecture and Civil Engineering, City University of Hong Kong,
- 7 Hong Kong, China
- 8 ° College of Hydraulic and Environmental Engineering, China Three Gorges University,
- 9 Yichang, China
- 10 d China Railway No.5 Engineering Group Co. Ltd, China

Abstract

11

12

13

14

15

16

17

18

19

20

Diamond nanothreads (DNT) and carbon nanotubes (CNT) have emerged as promising reinforcement materials for asphalt. However, the interfacial properties between DNT/CNT and asphalt remain poorly understood, hindering the advancement of DNT/CNT-modified asphalt nanocomposites. In this study, the pullout tests are conducted on asphalt nanocomposites reinforced with DNT, nitrogen-doped diamond nanothread (NDNT), and CNT, to analyze the pullout performance and reinforcing mechanisms across various temperature ranges. The findings reveal that CNT modified asphalt nanocomposites exhibit superior pullout performance compared to

^{*} Corresponding author. E-mail address: xfliu6-c@my.cityu.edu.hk (Xuefeng LIU).

Nanoscale Accepted Manuscript

1

4

5

6

7

8

9

13

14

15

16

17

18

19

20

21

those reinforced with DNT, primarily due to π - π stacking interactions that facilitate the

wrapping of asphalt molecules around the CNT surfaces. Among the DNT variants, 2

the DNT2 modified asphalt nanocomposite demonstrates the highest pullout 3

performance, attributed to its helical structure that enhances mechanical interlocking

within the asphalt matrix. Notably, NDNT shows the highest binding energy relative

to both DNTs and CNTs, stemming from interactions between hydroxyl groups on

asphaltene-phenol and nitrogen atoms on NDNT, leading to the formation of O-H···N

Density functional theory (DFT) calculations indicate that nitrogen hydrogen bonds.

doping modifies the electronic structure of NDNT, resulting in localized negative

10 charges that enhance its overall electronegativity.

Keywords: Asphalt; Interfacial properties; Diamond nanothread; Carbon nanotube; 11

12 DFT calculations.

1 Introduction

1.1 Background

While asphalt pavements offer advantages such as smooth and quiet surfaces, rapid construction, and simplified maintenance, their widespread application is constrained by the inherent thermomechanical properties of asphalt 1. The thermomechanical properties of asphalt refer to how its mechanical behavior changes in response to temperature variations ^{2, 3}. Poor thermomechanical properties lead to temperature-induced distress and fatigue cracking under loads and environmental impacts, necessitating frequent and costly maintenance that strains infrastructure

2

3

18

19

20

21

thermomechanical properties of asphalt through innovative material modification

strategies to enhance the long-term durability of asphalt pavement.

budgets and disrupts traffic.

View Article Online

Therefore, it is imperative to improve the

modification methods, the introduction of nanomaterials offers a promising alternative.

The unique physical and chemical properties of nanomaterials provide significant

advantages in enhancing the performance of asphalt, making them an attractive option

for future research and application 9. Nanomaterials, particularly carbon-based

View Article Online

like nano-clay, nano-silica, and nano-TiO₂, exhibit exceptional mechanical properties,

1

2

21

materials such as carbon nanotubes (CNTs) and graphene, as well as inorganic materials

up to 2000 W/m·K, which facilitates an even distribution of pavement temperature.

This, in turn, helps to minimize thermal stress concentrations and lowers the risk of 1 cold cracking of asphalt. Furthermore, the hydrogenated surfaces facilitate covalent 2 bonding between DNTs and matrix, allowing for their functionalization without 3 introducing any defect in the backbone structure, making them especially suitable as 4 modifiers for nanocomposites ^{17, 18}. In particular, nitrogen-doped diamond nanothread 5 (NDNT) enhances the interfacial interactions due to its unique surface properties, which 6 7 improve adhesion with the asphalt matrix. The surface chemistry of DNT, NDNT, and CNT is fundamentally different, leading to variations in interfacial adhesion. 8 9 Enhanced interfacial adhesion is vital for preventing debonding and ensuring effective 10 stress transfer throughout the modified material. The complexity of asphalt molecules has hindered a thorough understanding of how DNT, NDNT, and CNT reinforce the 11 12 interfacial properties of asphalt nanocomposites. While previous studies have 13 primarily concentrated on the individual effects of CNTs on asphalt properties, our 14 research uniquely explores the interfacial load transfer capabilities and shear resistance of both DNT and CNT modified asphalt for the first time. To the best of the authors' 15 16 knowledge, few studies have clarified the reinforcing mechanisms of DNT, NDNT, and CNT within the asphalt matrix at the atomistic level. The unveiled mechanisms are 17 crucial for understanding the unique interactions between the reinforcements and 18 19 asphalt, which can aid in predicting and optimizing the performance of DNT modified 20 asphalt nanocomposites.

Nanoscale Accepted Manuscript

1.3 Research motivation

1

2

3

4

5

6

7

8

9

10

11

12

13

14

15

16

17

18

19

20

21

Experimentally investigating DNT/CNT reinforced asphalt at the nanoscale is difficult due to the challenges in manipulating and observing nanoscale interactions in the laboratory. Molecular dynamics (MD) simulations provide a powerful and advantageous alternative ^{19, 20}. MD simulations are widely employed to investigate the interfacial behaviors and mechanical properties of DNT/CNT modified materials due to the atomistic resolution and ability to capture molecular interactions. MD simulations have been utilized to study the interfacial contact behaviors between CNTs and asphalt binders, revealing that the addition of multi-walled CNTs can significantly enhance the adhesion ability of asphalt on aggregate surfaces, particularly for alkaline The effects of DNT on the glass transition temperature of poly(methyl methacrylate) (PMMA) composites are investigated by MD simulations, demonstrating the exceptionally high glass transition temperatures and low densities of DNT modified PMMA composites ²². Besides, MD simulations and DFT calculations are combined to explore the frictional performance of DNT modified polymer composites, underscoring that DNT significantly enhances the frictional resistance of polymer composites by the improved interfacial interactions ²³. Furthermore, MD simulation overcomes the experimental limitations by enabling the direct visualization and quantification of interactions at the atomistic level, providing atomistic insight into the reinforcement mechanisms between asphalt and DNT/CNT ²⁴⁻³¹. While asphalt consists of complex and diverse components, MD simulation can effectively manage

View Article Online

this complexity and offer insights into the interactions between DNT/CNT and asphalt

molecules ^{32, 33}. Asphalt properties, including aging, fatigue cracking, and moisture resistance, have been detailly investigated by MD simulations, and the availability and validity of MD can be demonstrated ^{6, 34, 35}. Additionally, MD simulations have demonstrated the ability to assess the mechanical strength, thermal conductivity, and interfacial adhesion of DNT/CNT nanomaterials ^{36,37}. Compared to the high costs and time investments associated with nanoscale experiments, MD offers a more cost-effective and efficient approach to explore a broader range of parameters and predict the performance of DNT modified asphalt, thus accelerating the development of

1.4 Research objective

optimized asphalt nanocomposites.

The objective of this study is to investigate the shear resistance of DNT/CNT modified asphalt nanocomposites, comparing the reinforcing mechanisms between DNT and CNT in asphalt nanocomposites at the first time. Pullout tests are employed to assess the interfacial load transfer capabilities between asphalt and DNT/CNT, while DFT calculations are applied to examine the interfacial binding and electrostatic properties. Results show that the uneven hydrogenated surface of DNT creates geometric restrictions with asphalt matrix, facilitating the mechanical interlocking and reducing the mobility of asphalt along the longitudinal direction of DNT, thereby enhancing load transfer. Hydrogen bonding increases the shear resistance of NDNT by constraining molecular motion of asphalt molecules within the matrix. The

Nanoscale Accepted Manuscript

10

11

12

13

14

15

16

17

18

19

20

21

1

due to the polarized nitrogen-doping surface. In contrast, CNT modified asphalt 2 nanocomposites exhibit higher resistance to shear deformation and increased rigidity 3 The π - π stacking interactions are crucial, allowing asphalt molecules to 4 than DNTs. 5 wrap around CNT surfaces, which improves adhesion and load transfer. The delocalized π -electrons of CNT enhance adhesion with aromatic rings in asphalt. By 6 assessing the effectiveness of DNTs and CNTs in asphalt nanocomposites, this study 7 uncovers new strategies for developing more efficient nanomaterials for asphalt 8 9 reinforcement, which can significantly enhance the durability and lifespan of asphalt

2 Model and methodology

2.1 Atomistic model

pavement.

The 12-molecule model representing AAA-1 asphalt from the Strategic Highway Research Program (SHRP) asphalt systems is employed in this study, which has been widely adopted in asphalt research ³⁸. Four components, including asphaltene, polar aromatics, naphthene aromatics, and saturates, are identified in this model, as shown in Figure 1(a). Each component consists of several representative molecules, which are determined by the Hansen solubility parameters and mass fractions of the corresponding elements and components in asphalt ³⁹. Three molecular structures, namely asphaltene-phenol, asphaltene-pyrrole, and asphaltene-thiophene, are chosen to represent asphaltene molecules, as they more accurately reflect the true asphaltenes and

2

3

4

5

6

7

8

9

10

11

12

13

14

15

16

17

18

19

20

21

View Article Online mitigate the "pentane effect" ⁴⁰. The polar aromatics are represented by five different molecules from the sedimentary rock samples of geochemistry literature, including quinolinohopane, thioisorenieratane, benzobisbenzothiophene, pyridinohopane, and Two naphthene aromatic molecules are identified in this trimethylbenzeneoxane 41. model as perhydrophenanthrene-naphthalene (PHPN) and dioctyl-cyclohexanenaphthalene (DOCHN), possessing the average distribution of aromatic, naphthenic and paraffinic carbons of crude oils. Finally, hopane and squalene are selected as the saturate components of asphalt, aligning with the direct separation and quantitative analysis of n- and iso-alkanes in neat SHRP asphalts. Hopane is typically found in crude oils, while squalene is derived from both plant and animal sources and is also present in petroleum ⁴². The molecular formula and fractions of different asphalt components are presented in Table 1. The mass ratios of four components in the asphalt model are calculated and shown in Figure 2, which is in good accordance with the asphalt from the experimental measurement ³⁹. The molecular mass ratios help determine the balance between the reinforcing capabilities of the nanomaterials and the viscosity of the asphalt, which is essential for ensuring optimal dispersion and interaction within the nanocomposite. The number of each type of molecule used in our model asphalts was carefully adjusted to align with experimental data on asphalt speciation and atomic composition from SHRP asphalts ³⁹. This approach ensures that our model accurately represents the complex composition of real-world asphalt, which typically contains a balance of various sizes and atom types, including carbon,

Nanoscale Accepted Manuscript

hydrogen, nitrogen, sulfur, and oxygen ⁴³. Various stable DNT topologies have been Various stable DNT topologies have been 1 found by the first-principle calculations, which can be synthesized and characterized 2 using experimental methods ⁴⁴. Three typical DNTs with the same aspect ratios are 3 selected and identified as DNT1, DNT2, and DNT3 in this study, as shown in Figure 4 These DNTs exhibit sp³ hybridization and are present in their lowest energy 5 DNT1 is derived from a hydrogenated carbon nanotube with a chirality of (3, 6 0), known for its stability and favorable electronic properties. DNT2 features a coiled 7 structure, providing insights into how curvature affects mechanical properties and 8 9 interactions with surrounding materials. DNT3 adopts a zigzag configuration, 10 allowing us to explore the effects of this topology on the overall performance and compatibility with asphalt. Each of these structures exhibits sp³ hybridization and is 11 present in its lowest energy state, making them suitable candidates for our 12 13 investigations. Besides, NDNT is proposed to investigate the influence of 14 heteroatoms on DNTs interacting with asphalt. NDNT is constructed by substituting the carbon atoms on certain locations of the nanothread backbone by nitrogen atoms, 15 and the nitrogen ratio of NDNT model is 16.7% to ensure adequate dopants 45. 16 17 Furthermore, a molecular structure of CNT with a chirality of (3, 0) is also constructed 18 to compare with the DNT and NDNT structures with the same aspect ratio. 19 length and aspect ratios of DNT, NDNT, and CNT are chosen to ensure a fair 20 comparison in the pullout test.

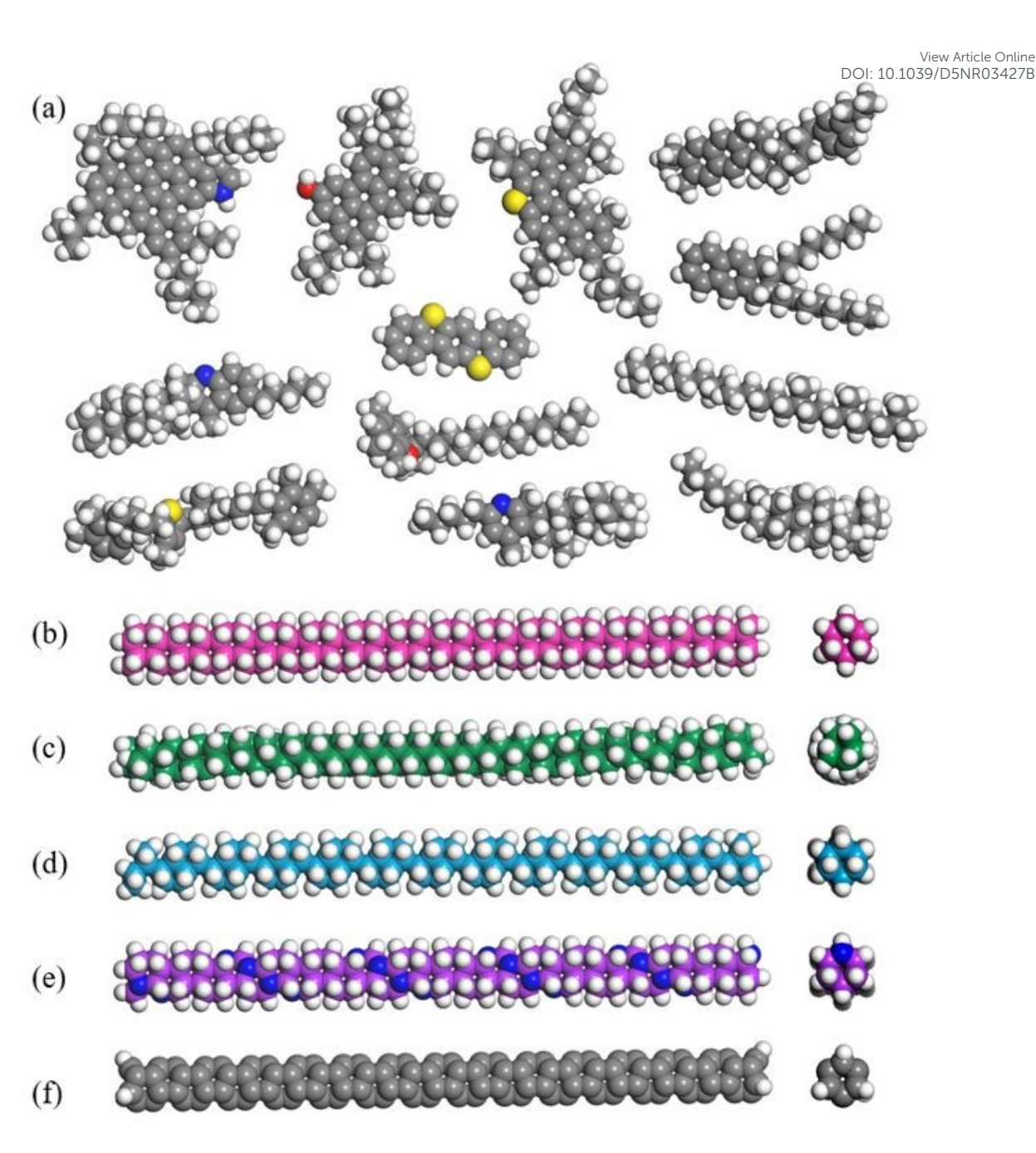


Figure 1 Atomistic configurations of (a) 12-molecule asphalt model. Front views and

3 side views of (b) DNT1, (c) DNT2, (d) DNT3, (e) NDNT, and (f) CNT with chirality

4 of (3, 0). (The dark blue atoms on NDNT refer to the doped nitrogen atoms).

5

1

2

View Article Online DOI: 10.1039/D5NR03427B

Open Access Article. Published on 28 2025. Downloaded on 02.11.2025 20:14:45.

This article is licensed under a Creative Commons Attribution-NonCommercial 3.0 Unported Licence.

Table 1 Molecular formula and ratios of asphalt components.

		Molecular	Number	Molecular	Mass
Component	Molecular type	formula		mass	ratio
		iormuia		(g/mol)	(%)
	Asphaltene-phenol	C ₄₂ H ₅₄ O	12	574.9	5.3
Asphaltene	Asphaltene-pyrrole	$C_{66}H_{81}N$	8	888.4	5.5
	Asphaltene-thiophene	$C_{51}H_{62}S$	12	707.1	6.5
	Quinolinohopane	$C_{40}H_{59}N$	16	553.9	6.8
D 1	Thioisorenieratane	$C_{40}H_{60}S$	16	573.0	7.0
Polar	Benzobisbenzothiophene	$C_{18}H_{10}S_2$	60	290.4	13.4
aromatics	Pyridinohopane	$C_{36}H_{57}N$	16	503.9	6.2
	Trimethylbenzeneoxane	$C_{29}H_{50}O$	20	414.7	6.4
Naphthene	PHPN	$C_{35}H_{44}$	44	464.7	15.7
aromatics	DOCHN	$C_{30}H_{46}$	52	406.7	16.2
S-4 4	Hopane	$C_{30}H_{62}$	16	482.9	5.9
Saturate	Squalane	$C_{35}H_{62}$	16	422.8	5.2

View Article Online DOI: 10.1039/D5NR03427B

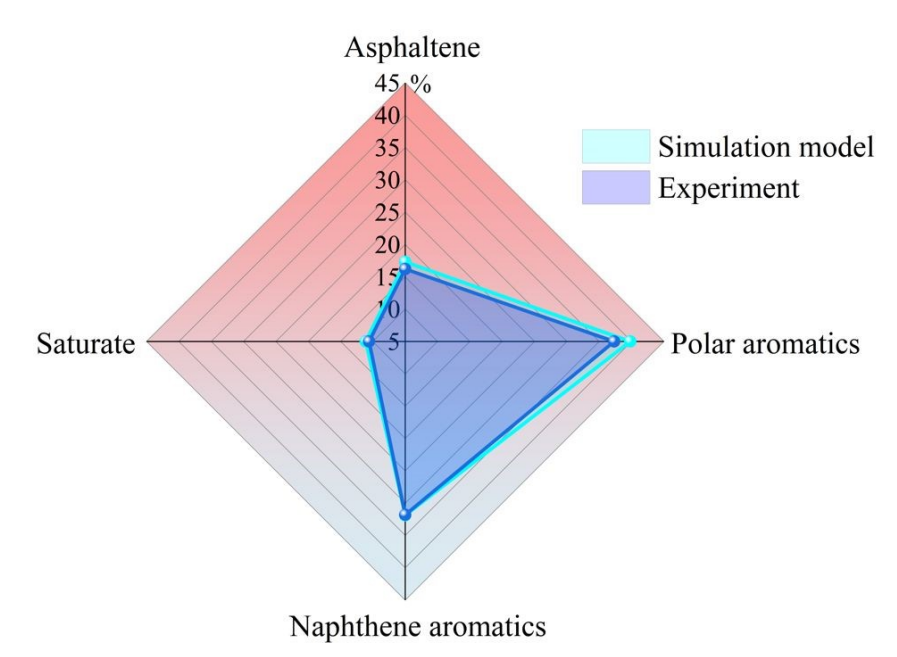


Figure 2 Mass ratios of four asphalt components between model and experiment.

2.2 Forcefield

In this study, we applied the Consistent Valence Forcefield (CVFF) for the MD simulations due to its broad applicability and proven effectiveness in accurately modeling molecular interactions in asphalt and CNT based nanomaterials. Although CVFF might have limitations in modeling highly specific hydrogen bonding or other nuanced interactions compared to COMPASS or PCFF forcefield, it is capable of reliably calculating essential physical and mechanical properties of asphalt, including density, cohesive energy density, and diffusion coefficient, which are crucial for understanding the behavior of asphalt in various applications ^{46, 47}. Furthermore, CVFF has been successfully employed to investigate the mechanical properties of CNTs and DNTs, capturing their unique bonding characteristics and structural behaviors ^{48, 49}. Additionally, CVFF is well-suited for MD simulations because it

Nanoscale Accepted Manuscript

11

12

- 2 simulations accurately reflect the dynamic behaviors of nanocomposites ⁵⁰. The
- 3 functional expression of CVFF is presented as:

$$E_{total} = \sum_{b} K_{b} (b - b_{0})^{2} + \sum_{\theta} K_{\theta} (\theta - \theta_{0})^{2} + \sum_{\phi} K_{\phi} [1 + s \cos(n\phi)] + \sum_{\chi} K_{\chi} [1 - \cos(2\chi)]$$

$$+ \sum_{nonbond} \left\{ \varepsilon_{ij} \left[\left(\frac{r_{ij}^{o}}{r_{ij}} \right)^{12} - \left(\frac{r_{ij}^{o}}{r_{ij}} \right)^{6} \right] + \frac{q_{i}q_{j}}{\varepsilon_{0}r_{ij}} \right\}$$

$$(1)$$

- 5 Here, the energy terms are composed of the bonded interaction terms and the non-bond
- 6 interaction terms. The bonded interaction terms involve bond interactions, bond angle
- interactions, torsional angle interactions, and out-of-plane angle interactions. 7 The
- 8 non-bond interaction terms involve the van der Waals interactions and the electrostatic
- 9 The van der Waals interactions are represented by the LJ-12-6 function,
- 10 while the electrostatic interactions are described by the Coulombic function.

2.3 Simulation method

13 The adopted asphalt model and forcefield are validated by computing the key properties, including density, viscosity, and glass transition temperature $(T_{\rm g})$. 14 15 density values are obtained from the simulation results after a 1-ns NPT simulation at 16 300 K and 101 kPa, once the asphalt system reaches full equilibrium. method ⁵¹ is a precise and effective way to determine the shear viscosity of the asphalt 17 18 system, and the formula is shown below:

$$\eta = \frac{V}{\kappa_{_{B}}T} \int_{0}^{\infty} \left\langle P_{\alpha\beta}^{S}(0) P_{\alpha\beta}^{S}(t) \right\rangle dt \tag{2}$$

Open Access Article. Published on 28 2025. Downloaded on 02.11.2025 20:14:45.

[6c] BY-NO This article is licensed under a Creative Commons Attribution-NonCommercial 3.0 Unported Licence.

View Article Online where η refers to the viscosity of asphalt, κ_B refers to the Boltzmann constant, V and 1 $P_{\alpha\beta}^{S}(0)$ and $P_{\alpha\beta}^{S}(t)$ T are the volume and temperature of the system, respectively. 2 are the instantaneous values of the off-diagonal stress tensor components $\alpha\beta$ at the 3 initial time and at a specific time of t, respectively. The glass transition temperature 4 represents the motion characteristics of polymeric materials, specifically referring to 5 the mobility of molecular chains ⁵². The glass transition temperature of the asphalt 6 system is determined using a stepwise cooling approach within molecular dynamics 7 simulations. Initially, the system is equilibrated at 420K for 1 ns under NPT 8 9 conditions (1 fs timestep, Nose-Hoover thermostat/barostat). The temperature is then 10 lowered in 20K decrements to 100K. Each cooling step involves a 150-ps NPT simulation, comprising a 50-ps cooling phase and a 100-ps equilibration period. 11 12 specific volume values at each temperature are averaged and recorded. Three 13 independent simulations are performed to ensure statistical accuracy. 14 The pullout test is conducted to investigate the shear resistance and interfacial interactions between asphalt and DNTs, as depicted in Figure 3. Before the pullout 15 16 process, both DNT and CNT structures undergo a thorough equilibration procedure, including initial optimization using a 500-ps NPT ensemble at 300K and 101kPa, 17 18 followed by the application of nonperiodic boundary conditions along the length 19 direction with a 120Å vacuum gap. A further 200-ps NVT ensemble at 300K is 20 applied for additional relaxation, simulating realistic conditions during the interaction 21 of DNT/CNT with asphalt. The dragged end of the reinforcement is considered rigid,

NVT ensemble, while the lateral edges of the 10Å thick asphalt are kept fixed. 3

pullout velocity is chosen based on the previous pullout speed of CNT from the asphalt 4

matrix, which can lead to reasonable results ⁵³. The pullout simulation results are 5

averaged across multiple independent configurations to minimize the random error.

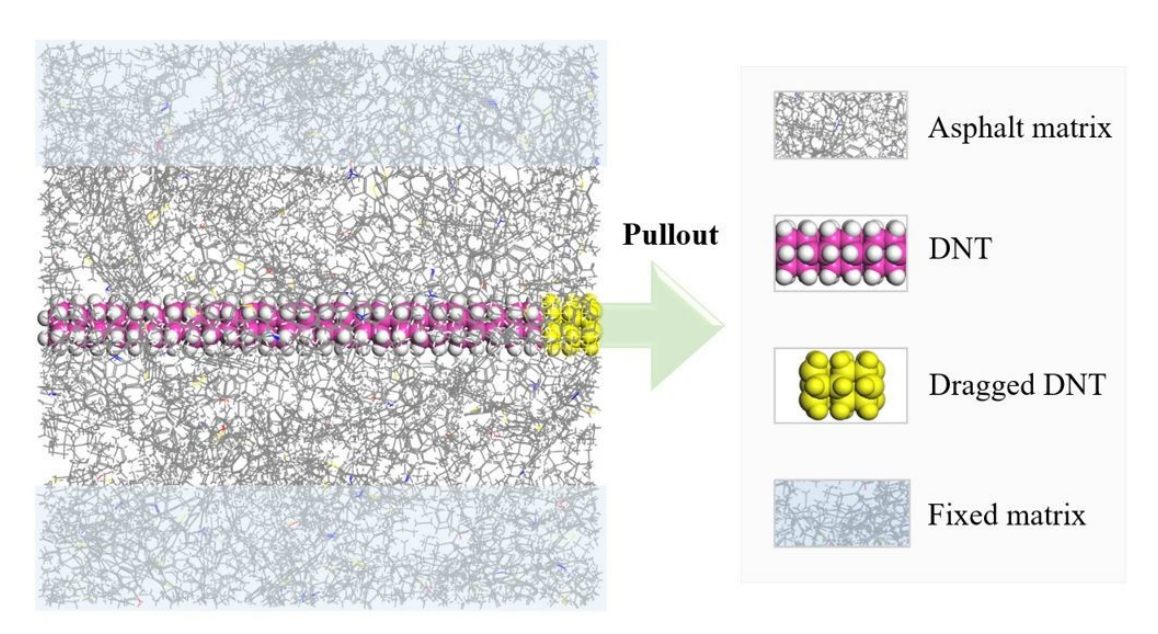


Figure 3 Diagram of DNT pulled out from asphalt matrix.

9

10

11

12

13

14

15

7

8

6

This article is licensed under a Creative Commons Attribution-NonCommercial 3.0 Unported Licence.

Open Access Article. Published on 28 2025. Downloaded on 02.11.2025 20:14:45.

The binding energy and molecular electrostatic potential are computed to investigate the interaction difference between asphalt components and reinforcements. The molecular electrostatic potentials between asphalt and reinforcements are accurately computed using density functional theory(DFT). For these calculations, the generalized gradient-corrected functionals of Perdew-Burke-Ernzerhof(PBE) are applied to assess the electronic properties. The atomic orbital basis set is defined

using double numerical plus d-functions, with a global orbital cutoff radius set at 3.3

- 2 Å. Geometry optimization and DFT calculations are performed using the DMol3
- 3 module in Materials Studio, with an energy convergence tolerance of 0.001Ha, a
- 4 maximal force of 0.02Ha/Å, and a maximal displacement of 0.001Å. Incorporating
- 5 dispersion corrections would increase both the complexity and computation time of our
- 6 DFT calculations; therefore, they are not included to maintain computational efficiency
- Additionally, since asphalt and reinforcement materials primarily rely on polar and
- 8 electrostatic interactions rather than dispersion forces, the necessity for dispersion
- 9 corrections is less critical 55. The formula of binding energy(E_{Bind}) is presented as:

$$E_{\text{Bind}} = E_{\text{Asphalt-reinforcement}} - E_{\text{Asphalt}} - E_{\text{Reinforcement}}$$
 (3)

- Where $E_{Asphalt-reinforcement}$ refers to the total energy of the asphalt and reinforcement
- system, $E_{Asphalt}$ and $E_{Reinforcement}$ refer to the energy of the isolated asphalt and the
- isolated reinforcement, respectively.
- The scheme of atomistic modeling and methodology is shown in Figure 4.

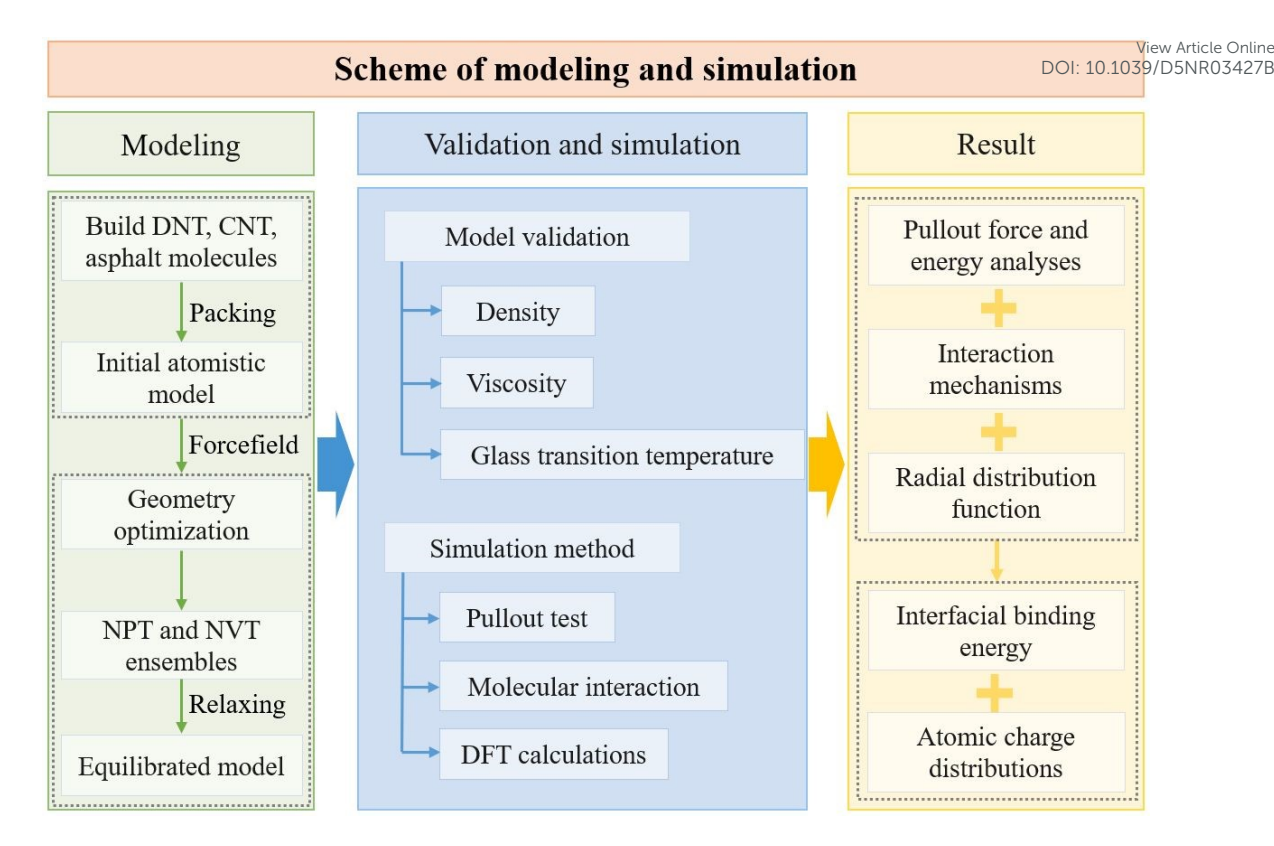


Figure 4 Scheme of atomistic modeling and simulation.

3 Results and Discussion

3.1 Model validation

The calculated density values of DNT1, DNT2, DNT3, NDNT, and CNT modified asphalt nanocomposites are all 1.01 g/cm³. The density value of pure asphalt is 1.02 g/cm³, showing a 2% deviation from the experimental value of approximately 1.0 g/cm³ ^{39, 56}. The density values of DNT/CNT modified asphalt nanocomposites are slightly lower than that of pure asphalt, indicating the lightweight feature of DNT/CNT modified nanocomposites. The viscosity of pure asphalt, DNT1 modified asphalt nanocomposite, DNT2 modified asphalt nanocomposite, DNT3 modified asphalt nanocomposite, NDNT modified asphalt nanocomposite, and CNT modified asphalt

3

4

5

6

7

8

9

10

11

12

13

14

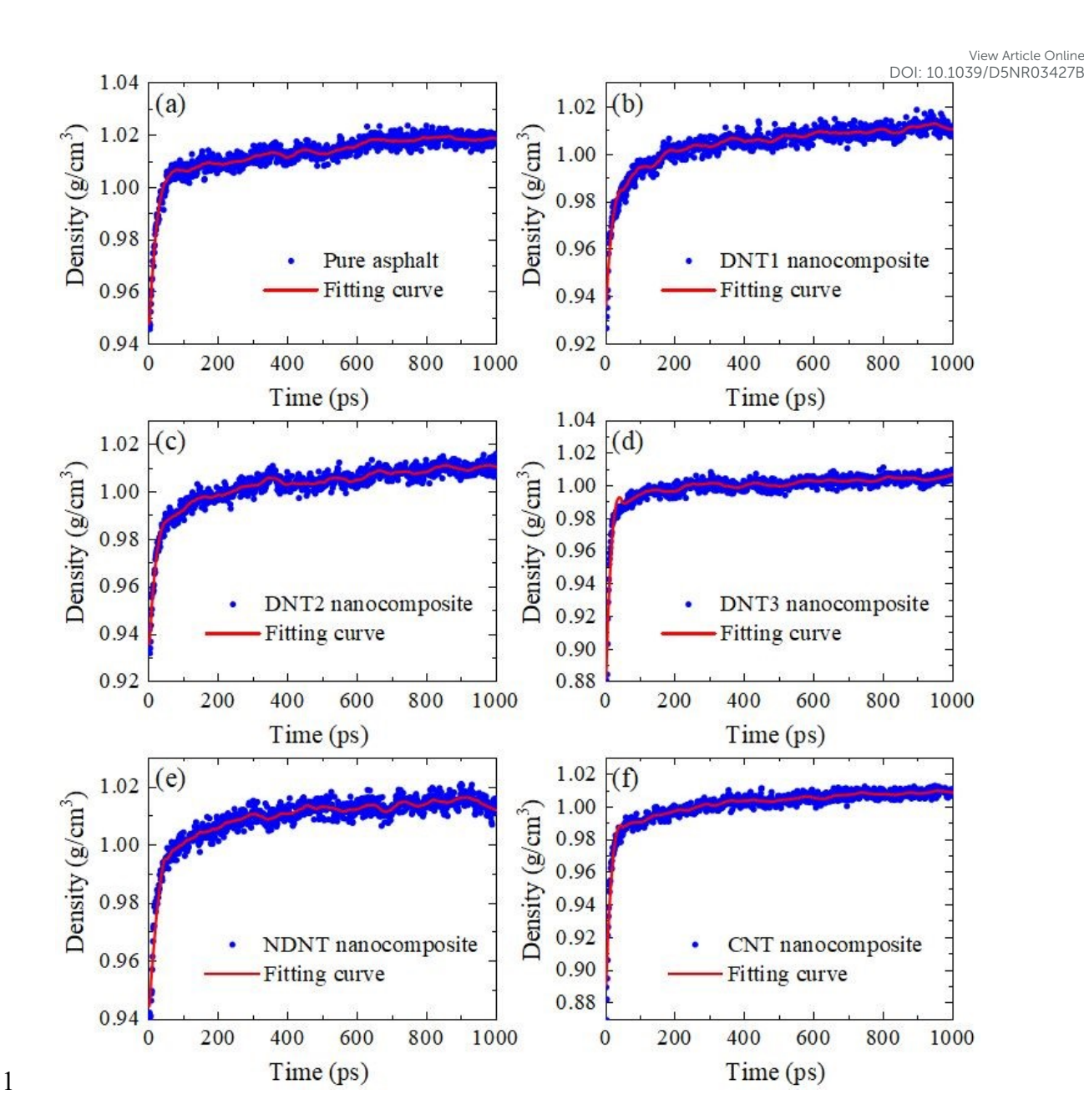
15

16

17

1 nanocomposite are 1.46 cP, 1.79 cP, 1.72 cP, 1.53 cP, 2.09 cP, and 2.15 cP, respectively.

The calculated viscosity is 1.46 cP, which deviates by about 3% from the viscosity result of 1.5 cP for the AAA-1 asphalt system ⁵⁷. It is found that DNT/CNT reinforcements can significantly increase the viscosity of asphalt, attributing to the increased interactions between DNT/CNT and asphalt matrix. The calculated $T_{\rm g}$ values of pure asphalt, DNT1 modified asphalt nanocomposite, DNT2 modified asphalt nanocomposite, DNT3 modified asphalt nanocomposite, NDNT modified asphalt nanocomposite, and CNT modified asphalt nanocomposite are 246K, 254K, 251K, 260K, 275K, and 255K, respectively. The calculated $T_{\rm g}$ value is 246 K, with a deviation of approximately 1% from the experimental $T_{\rm g}$ of 248.56 K for the AAA-1 asphalt system 52 . Compared to pure asphalt, the improved $T_{\rm g}$ values of DNT/CNT modified asphalt nanocomposites indicate the enhanced thermal stability and better deformation resistance to temperature fluctuations. Notably, NDNT modified asphalt nanocomposite has higher viscosity and T_g values than other DNTs. It is reckoned that nitrogen dopants of DNT structures play a positive role in the overall network strength and stability of DNT modified asphalt nanocomposites.



2 Figure 5 Density values of (a) pure asphalt, (b) DNT1 modified asphalt nanocomposite,

- (c) DNT2 modified asphalt nanocomposite, (d) DNT3 modified asphalt nanocomposite,
- 4 (e) NDNT modified asphalt nanocomposite, (f) CNT modified asphalt nanocomposite
- 5 during the equilibrium process.

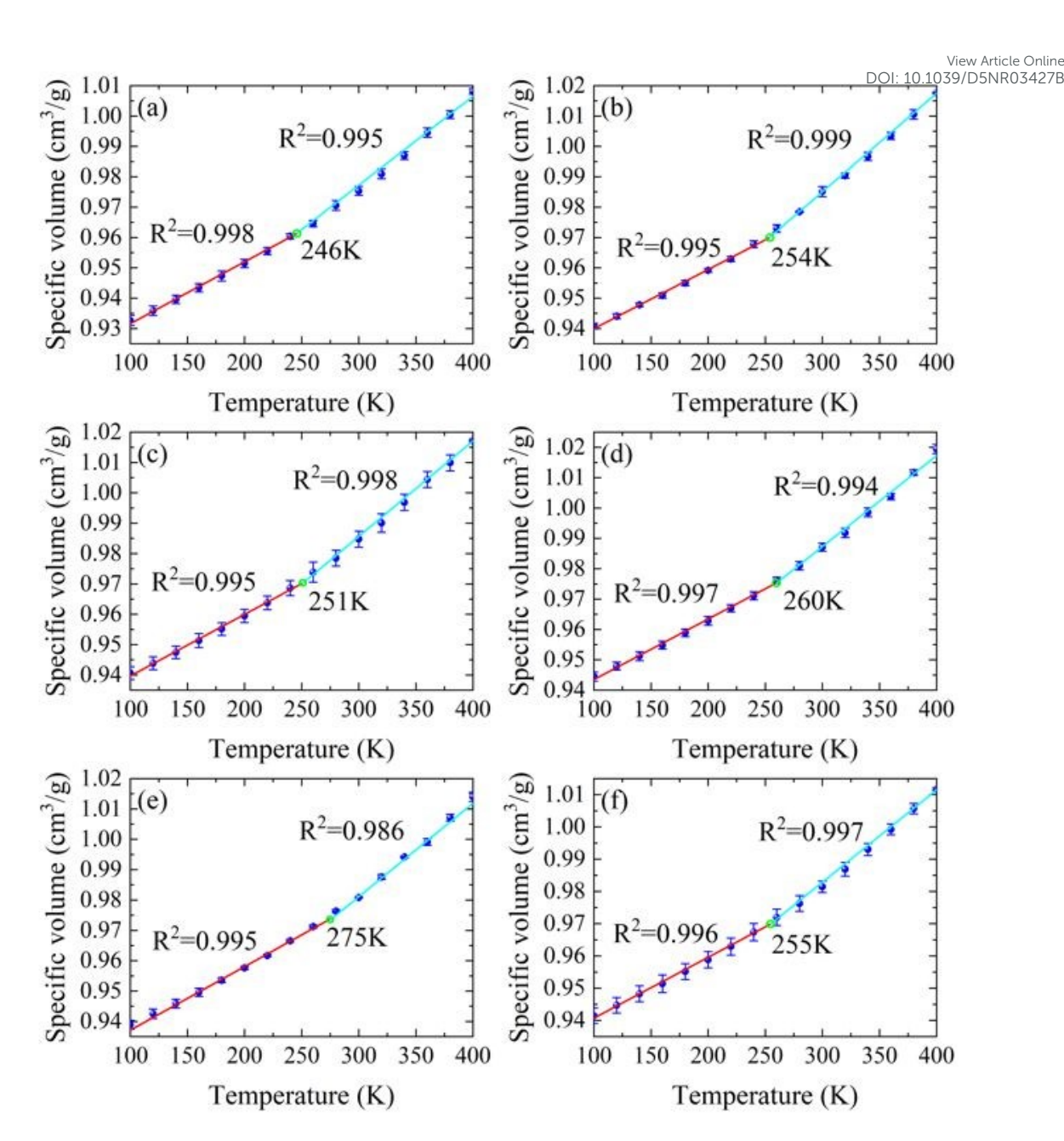


Figure 6 Specific volume values of (a) pure asphalt, (b) DNT1 modified asphalt nanocomposite, (c) DNT2 modified asphalt nanocomposite, (d) DNT3 modified asphalt nanocomposite, (e) NDNT modified asphalt nanocomposite, and (f) CNT modified asphalt nanocomposite vary under different temperature ranges. The $T_{\rm g}$ values of DNT/CNT modified asphalt nanocomposites are relatively higher than those of pure asphalt, indicating the higher deformation resistance to temperature changes.

1

2

3

4

5

6

3.2 Pullout test

This article is licensed under a Creative Commons Attribution-NonCommercial 3.0 Unported Licence

Open Access Article. Published on 28 2025. Downloaded on 02.11.2025 20:14:45.

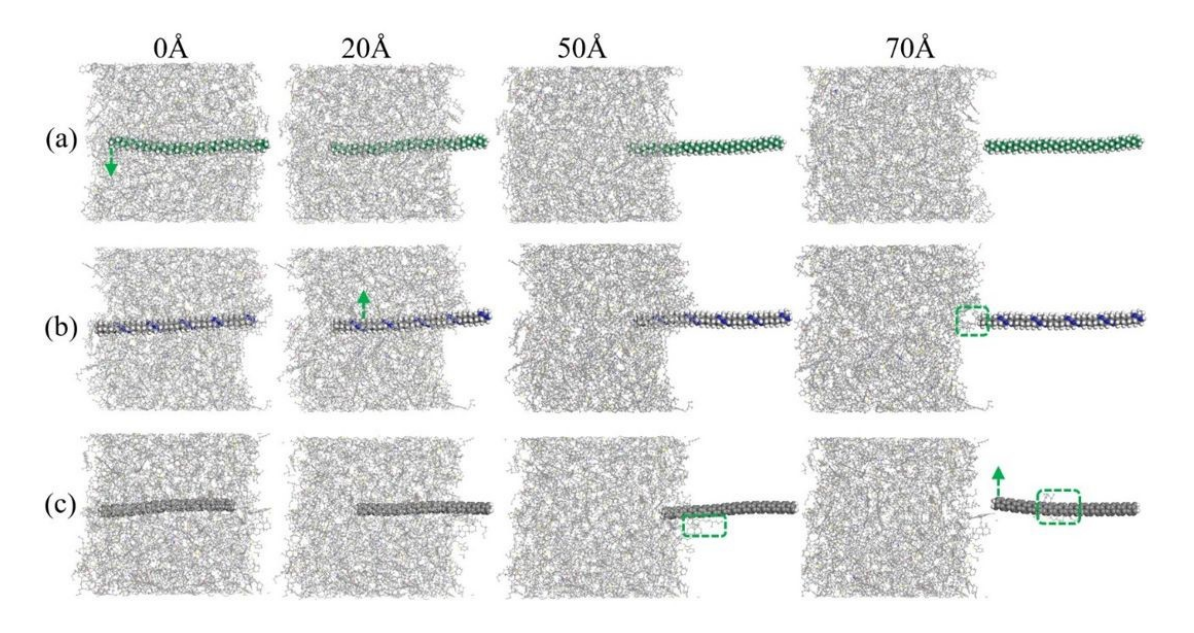


Figure 7 Snapshots of (a) DNT2, (b) NDNT, and (c) CNT pulled out from asphalt matrix.

The pullout tests are carried out to investigate the load transferring capability between DNT/CNT and asphalt matrix. The snapshots of DNT2, NDNT, and CNT pulled out from asphalt matrixes are depicted in Figure 7(a)-(c). It can be observed that the deformation occurs continuously perpendicular to the axial direction of DNT/CNT during the pullout process, while no noticeable deformation can be observed along the axial direction. All DNT/CNT structures with this aspect ratio exhibit high axial stiffness and significantly lower lateral stiffness, which makes them effective at transferring loads in the axial direction while being weaker laterally. During the pullout process, no asphalt molecules are extracted by the DNT, although a few asphalt chains bridge the interface between the NDNT and asphalt. In contrast, there is significantly more interaction between asphalt and CNT. Several asphalt molecules

3

4

5

6

7

8

9

10

11

12

13

14

15

16

17

18

19

20

21

adhere to the CNT surface before complete pullout, and some are transported away View Article Online

once the CNT is fully extracted. These close interactions highlight the strong

interfacial bonds and load-transfer capabilities between asphalt and CNT.

To quantitatively investigate the influence of different topological structures on the reinforcing capability, the pullout force values of DNT/CNT during the pullout process are calculated and depicted in Figure 8. The pullout displacement of DNT/CNT is recorded within 60Å, since the DNT/CNT is completely pulled out beyond 60Å. It can be observed that the pullout force of DNT/CNT increases rapidly at the initial stage and then fluctuates around a constant value. The root mean square (RMS) values of pullout force are extracted to quantitatively assess the pullout The RMS values of pullout force for DNT1, DNT2, performance of DNT/CNT. DNT3, NDNT, and CNT are 0.507nN, 0.514nN, 0.486nN, 0.511nN, and 0.575nN, respectively. It demonstrates that CNT modified asphalt nanocomposite possesses the highest pullout force among all the nanotubes, which echoes the findings that CNT has stronger interfacial interactions. The pullout force of DNT2 modified asphalt nanocomposite is the highest among the DNTs. The improved pullout performance of DNT2 is attributed to its helical structure, which enhances mechanical interlocking within the asphalt matrix and minimizes relative movement between the asphalt and The pullout force of NDNT is comparable to that of DNT2, whereas DNT3 DNT2. exhibits the lowest pullout force among all the DNT variants. Additionally, NDNT shows significantly higher pullout performance than DNT1, suggesting that the

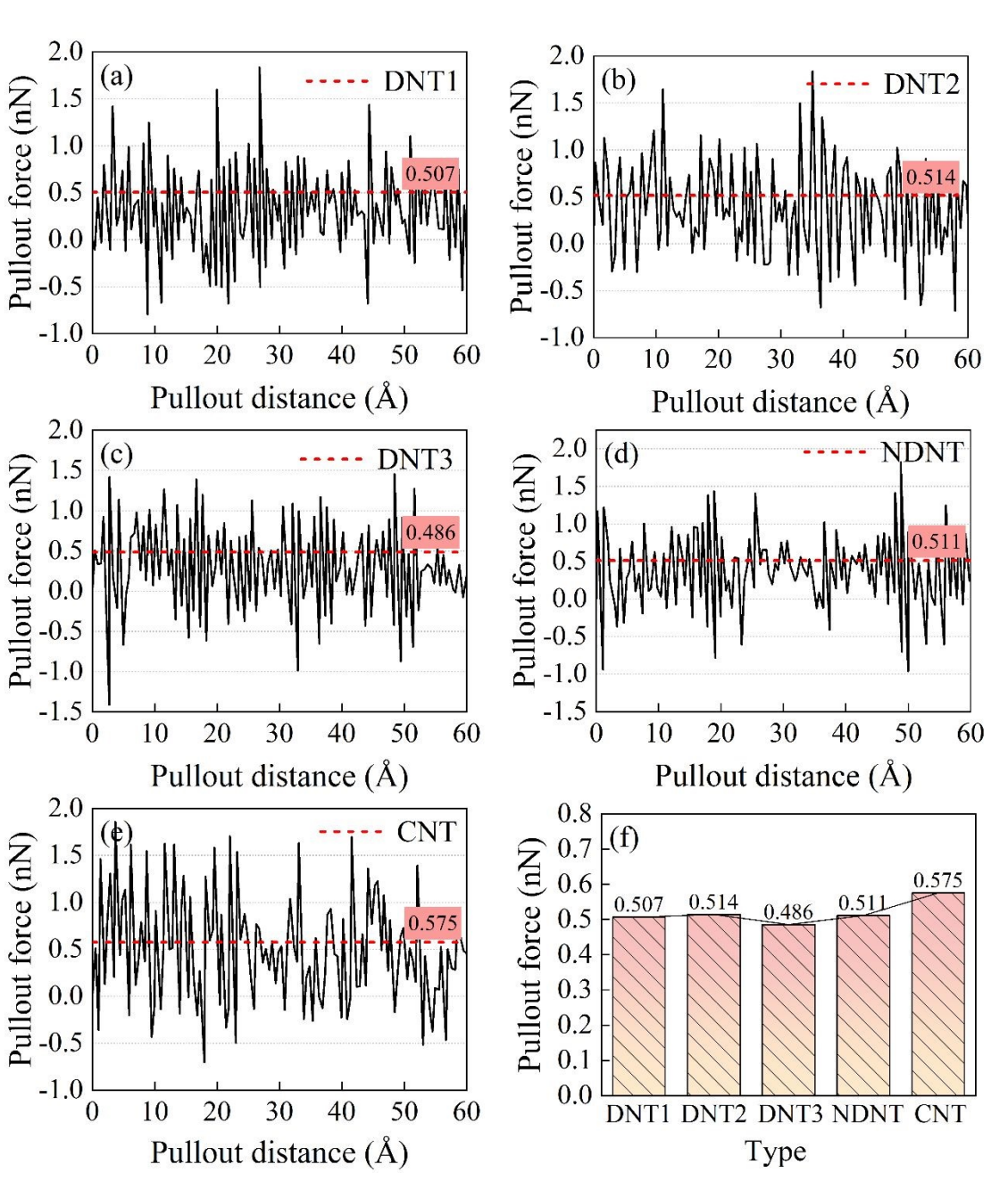
Nanoscale Accepted Manuscrip

1

3

6

7



4 Figure 8 Pullout force changes with the pullout distance during the pullout process.

5 (The red line indicates the RMS values of the data set).

The pullout energy curves of DNTs, NDNT, and CNT during the pullout process

are presented in Figure 9. The pullout energy of DNT/CNT steadily increases up to 1 60 Å, ultimately reaching its peak value, which refers to the complete extraction from 2 3 the asphalt matrix. The pullout energy of CNT is the highest, approximately 1.5 times greater than that of DNT2 and DNT3. The increased pullout energy reveals that the 4 CNT modified asphalt nanocomposite exhibits greater resistance to shear deformation, 5 contributing to its overall rigidity. The pullout energy of DNT2 is the highest among 6 the DNT reinforcements, which aligns with its significantly greater pullout force 7 discussed in the previous section. Meanwhile, the pullout energy of NDNT is slightly 8 9 lower than that of DNT2, but still surpasses that of DNT1 and DNT3. DNT3, with its 10 zigzag structure, exhibits the lowest pullout energy and load-transfer capacity within the asphalt matrix. Notably, the pullout energy of DNT3 is higher than that of DNT1 11 up to 47Å, but falls below that of DNT1 beyond this distance. 12 As demonstrated in 13 Figure 8, the pullout force of DNT3 decreases more rapidly when the pullout distance

exceeds 47Å, resulting in the lower pullout energy.

View Article Online

1

2

3

4

5

6

7

8

9

10

11

12

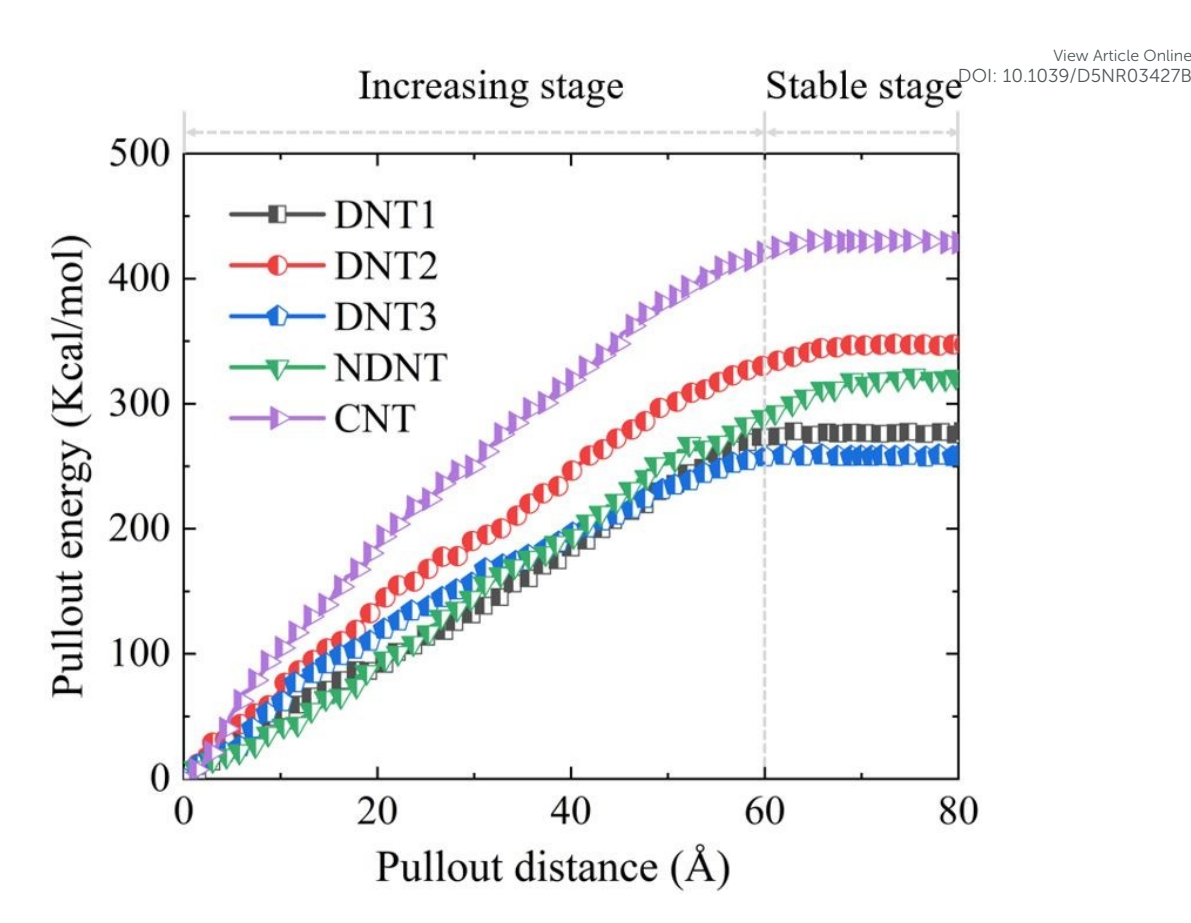


Figure 9 Pullout energy fluctuates with displacement during the pullout process.

The molecular interaction details at DNT and asphalt interfaces are demonstrated in Figure 10(a). It can be observed that the hydrogen atoms on the hydrogenated DNT surface can mechanically interlock with the asphalt atoms at the interface, which contributes to the shear resistance during the pullout process. A schematic representation of the interlocking effect between DNT and asphalt is depicted in Figure The uneven hydrogenated surface of DNT creates geometric constraints within the asphalt matrix, facilitating the mechanical interlocking interactions. This interaction reduces the mobility of asphalt along the longitudinal direction of the reinforcement, thereby enhancing mechanical interlocking and improving load transfer

View Article Online

The H-bond interaction capabilities between the DNT and the asphalt matrix. 1 between NDNT and asphaltene is presented in Figure 10(c). 2 It shows that the hydroxyl group on asphaltene-phenol can interact with the nitrogen atoms on NDNT to 3 generate the O-H···N H-bond. The H-bond interaction contributes to the enhanced 4 5 shear resistance of NDNT by increasing the motion constraints within the asphalt matrix, in contrast to DNTs without the nitrogen dopant. The π - π stacking interactions 6 between CNT and naphthene aromatic molecule(DOCHN) are presented in Figure 7 The π - π stacking interactions are crucial for enhancing the shear resistance of 8 9 asphalt, facilitating the wrapping of asphalt molecules around the surface of CNTs. 10 is found that the ratios of aromatic carbon can constitute up to 40% of the total carbon 11 content of asphalt, primarily derived from components including asphaltenes, polar 12 aromatics, and naphthene aromatics ³⁹. These molecules can generate a significant 13 number of π - π stacking interactions around CNTs, thereby enhancing the overall load 14 transfer capabilities of CNTs during the deformation and pullout process.

2

3

4

6

8

9

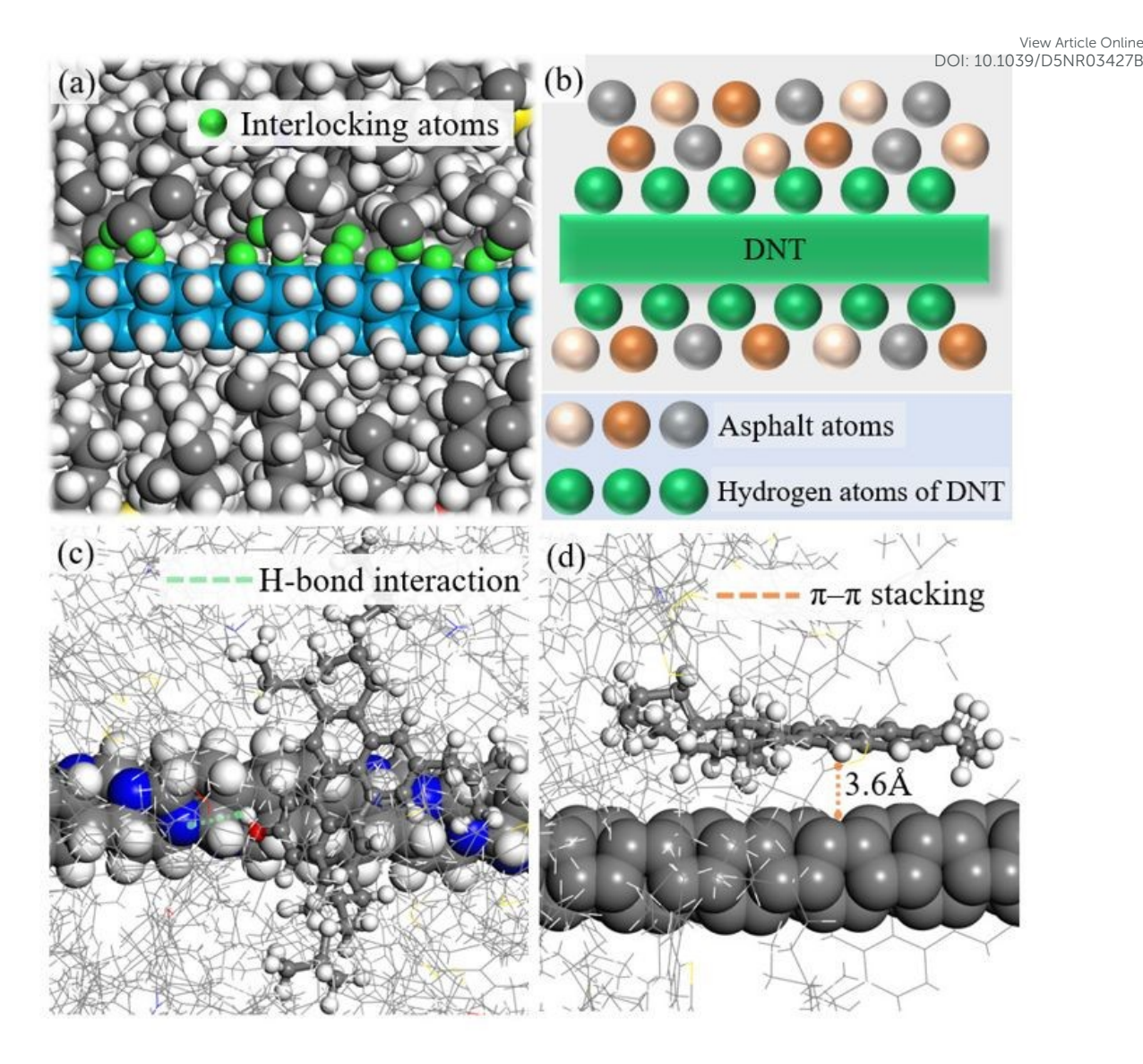


Figure 10 Molecular details between (a) DNT and asphalt interface; (b) Schematic illustration of interlocking effect at DNT-asphalt interface; (c) H-bond interaction between NDNT and asphaltene molecule; (d) π - π stacking interactions between CNT

5 and naphthene aromatic molecule.

7 The radial distribution function (RDF) curves between DNT/CNT and asphalt

components are depicted in Figure 11(a)-(c). It is noticeable that the g(r) values for

naphthene aromatics and DNTs peak within 8 Å, indicating stronger interactions

View Article Online

The molecular chains of naphthene aromatic molecules, including between the two. 1 2 DOCHN, can interact with the DNT surface through mechanical interlocking, leading to enhanced interactions. The g(r) curves between NDNT and asphalt molecules are 3 depicted in Figure 11(d). It is found that the g(r) values between saturate and NDNT 4 are higher than those of polar aromatics, asphaltene, and naphthene aromatics, 5 The chain-like structures of saturates can mechanically intertwine with respectively. 6 7 NDNT and enhance their interactions. Additionally, the nitrogen atoms on NDNT can engage in hydrogen bonding with the heteroatoms of asphaltenes and polar aromatics, 8 9 further enhancing these interactions. As illustrated in Figure 11(e), the g(r) values 10 between saturates and CNT are comparatively lower than those for other asphalt This suggests that CNT interacts more closely with asphaltenes, polar 11 12 aromatics, and naphthene aromatics, while exhibiting fewer active interactions with 13 saturate molecules. This discrepancy arises from CNT's enhanced interactions with 14 aromatic carbons through π - π stacking, which is a feature absent in saturate molecules. The RDF curves between DNT/CNT and asphalt are shown in Figure 11(f). 15 It demonstrates that DNTs and NDNT exhibit higher g(r) values than CNT within 3.6Å, 16 17 while showing lower values beyond this threshold. This divergence stems from the 18 distinct surface morphological characteristics between DNTs and CNT. The 19 hydrogenated surface of DNT engages more intimately with asphalt molecules through 20 mechanical interlocking, whereas π - π stacking interactions between CNT and asphalt 21 start to prevail at approximately 3.6Å. Notably, the g(r) values between CNT and

- asphalt are higher than those for DNTs and NDNT from 3.6Å to 16Å, suggesting View Article Online
- 2 stronger interactions between asphalt and CNT within this distance.

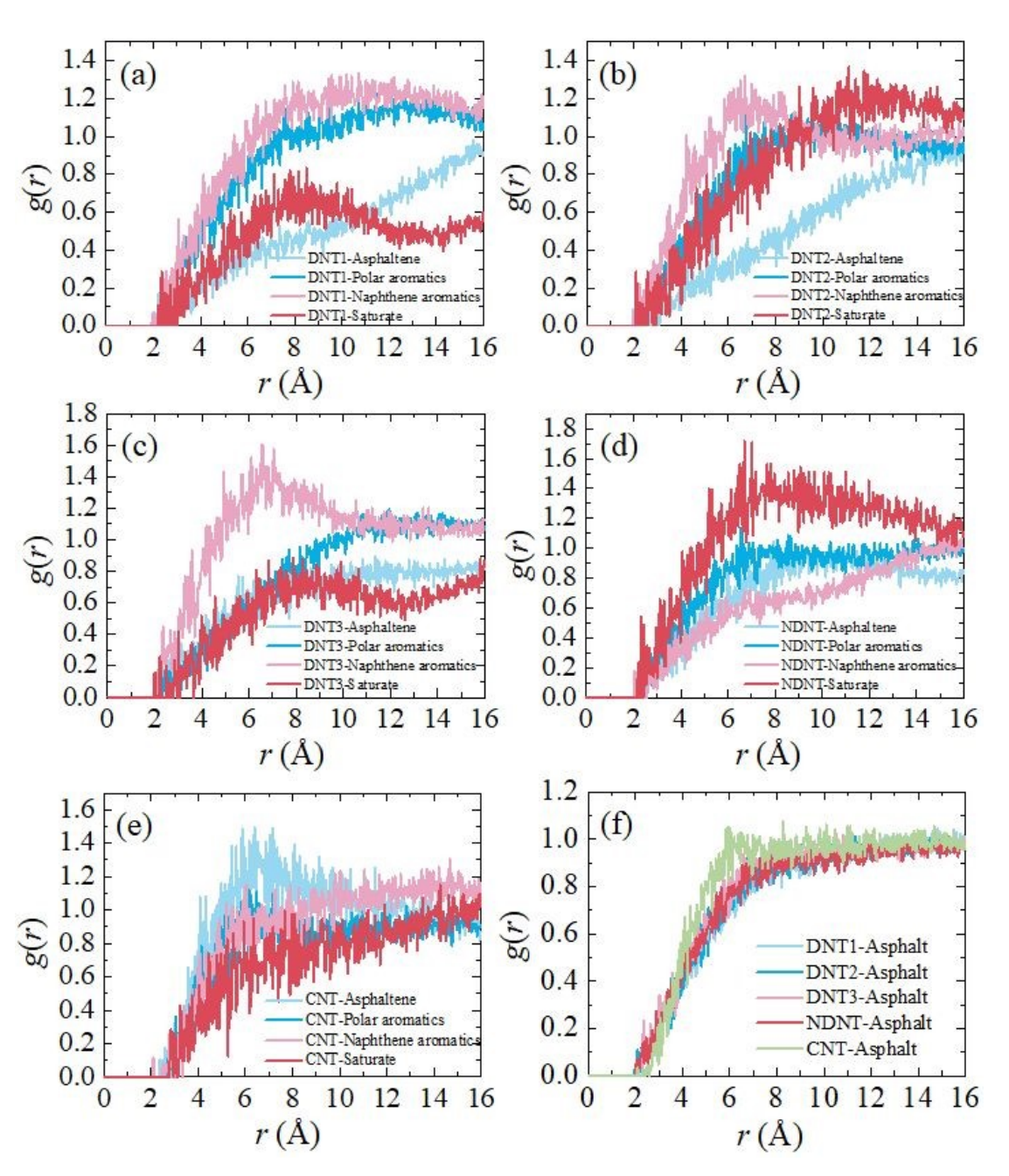


Figure 11 RDF curves between asphalt components and (a) DNT1, (b) DNT2, (c) DNT3,

- 5 (d) NDNT, and (e) CNT after the full equilibrium. (f) RDF curves between DNT/CNT
- 6 and asphalt molecules after the full equilibrium.

4

This article is licensed under a Creative Commons Attribution-NonCommercial 3.0 Unported Licence

Open Access Article. Published on 28 2025. Downloaded on 02.11.2025 20:14:45.

1

2

3

4

5

6

7

8

9

10

11

12

13

14

15

16

17

18

19

20

21

3.3 DFT calculation

Binding energy provides a quantitative measure of the interfacial interactions between asphalt and reinforcements ⁵⁸. The binding energy values between different asphalt components and DNT/CNT are presented in Figure 12. It shows that the binding energy values between polar components and DNT/CNT are relatively higher than those between nonpolar asphalt components and DNT/CNT. This indicates that the heteroatoms in the polar components of asphalt are essential for improving interfacial interactions with DNT/CNT. Among all asphalt components, the binding energy between asphaltene and DNT/CNT is the highest, primarily due to the larger molecular volume of asphaltene and the presence of heteroatoms. The binding energy values for DNT2 and DNT3 are the lowest among all components, with DNT2 showing an interaction of 13.7 Kcal/mol with saturates and DNT3 exhibiting 13.8 Kcal/mol with naphthene aromatics. NDNT achieves the highest binding energy with asphalt components, except for polar aromatics, where its value is slightly lower than that of The binding energy between NDNT and asphaltene is 55.8 Kcal/mol, CNT. comparatively higher than the 49.9 Kcal/mol observed for CNT and much greater than the 40 Kcal/mol for DNT1, 34.5 Kcal/mol for DNT2, and 35.7 Kcal/mol for DNT3. This increased binding energy is attributed to the presence of polarized nitrogen atoms in NDNT, which enhances the interfacial interactions between NDNT and asphalt The binding energy between CNT and asphalt is slightly lower than that of NDNT but significantly higher than that of DNTs. As previously mentioned, the

Nanoscale Accepted Manuscript

8

9

10

- aromatic rings in asphalt molecules can interact with CNT and adhere to its surface 1
- 2 through π - π stacking interactions, thereby enhancing interfacial interactions.
- Additionally, it has been observed that the binding energy values between DNT1 and 3
- asphalt molecules are the highest among the DNTs. DNT2 and DNT3 exhibit 4
- 5 significantly lower binding energy compared to others, indicating weaker interactions
- between asphalt molecules and DNT2/DNT3. 6 The reduced binding energy at the
- 7 DNT-asphalt interface can be ascribed to the hydrogen passivation of the DNT surface.

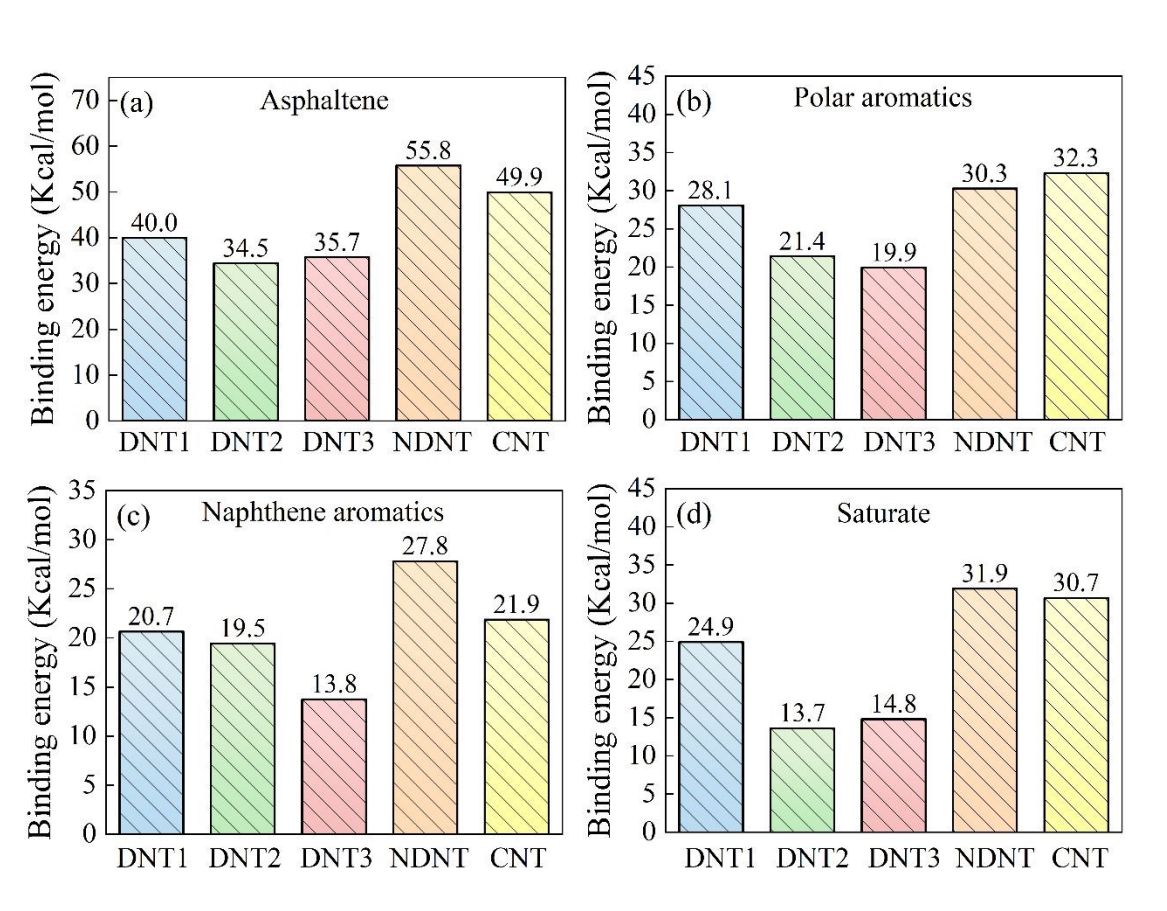


Figure 12 Binding energy between (a) asphaltene and DNT/CNT, (b) polar aromatics

- 11 and DNT/CNT, (c) naphthene aromatics and DNT/CNT, (d) saturate and DNT/CNT.
- 12 The binding energy between NDNT and asphalt components is relatively higher than
- 13 that of other DNTs, which is attributed to the polarized nitrogen-doped surface.

View Article Online DOI: 10.1039/D5NR03427B

2

3

4

5

6

7

8

9

10

11

12

13

14

15

16

17

18

19

20

21

Open Access Article. Published on 28 2025. Downloaded on 02.11.2025 20:14:45.

-NG This article is licensed under a Creative Commons Attribution-NonCommercial 3.0 Unported Licence.

The atomic charge distributions between asphalt and DNT/CNT are demonstrated through molecular electrostatic potential maps, which can provide detailed insights into the mechanisms underlying interfacial interactions. The molecular electrostatic potentials between DNT/CNT and asphalt molecules are calculated and depicted in The positive potential is denoted by the red color on the molecules, while Figure 13. the negative potential is represented by the blue color. As shown in Figure 13(a)-(c), DNTs exhibit the positive potential on the hydrogen atoms and the negative potential on the carbon atoms of the backbone, generating a relatively rough electrostatic potential map. The rough electrostatic potential of DNTs helps to create potential energy wells that trap the aliphatic chains of asphalt molecules, making it energetically unfavorable for them to move along the axis of DNTs. The interactions between DNTs and asphalt molecules are mainly governed by a combination of van der Waals forces, electrostatic attractions, and mechanical interlocking. In contrast to DNT, the presence of nitrogen dopants can alter the electronic structure of NDNT, as shown in Figure 13(d). This leads to the creation of localized negative charges, enhancing the overall electronegativity. It can be observed that the nitrogen atoms of NDNT exhibit strong negative potentials, while the hydrogen atom connected to the nitrogen atom on asphaltene exhibits strong positive potentials. The interactions between NDNT and asphaltene can be significantly enhanced by the attraction between the electropositive regions of asphaltene and the electronegative domain of NDNT. The strong

View Article Online

- 3 13(e), there are electronegative domains on the CNT surface but electropositive
- 4 domains on the ends of the hydrogen atoms on CNTs. The electrostatic potential on
- 5 CNT surface is comparatively smooth, since the delocalized π -electrons in the CNT
- 6 structure result in a more even distribution of electron density along the surface. The
- 7 delocalized π -electrons in CNTs can engage in π - π stacking interactions with the
- 8 aromatic rings in asphalt molecules, leading to stronger adhesion and load transfer
- 9 capability.

10

11

12

This article is licensed under a Creative Commons Attribution-NonCommercial 3.0 Unported Licence.

Open Access Article. Published on 28 2025. Downloaded on 02.11.2025 20:14:45.

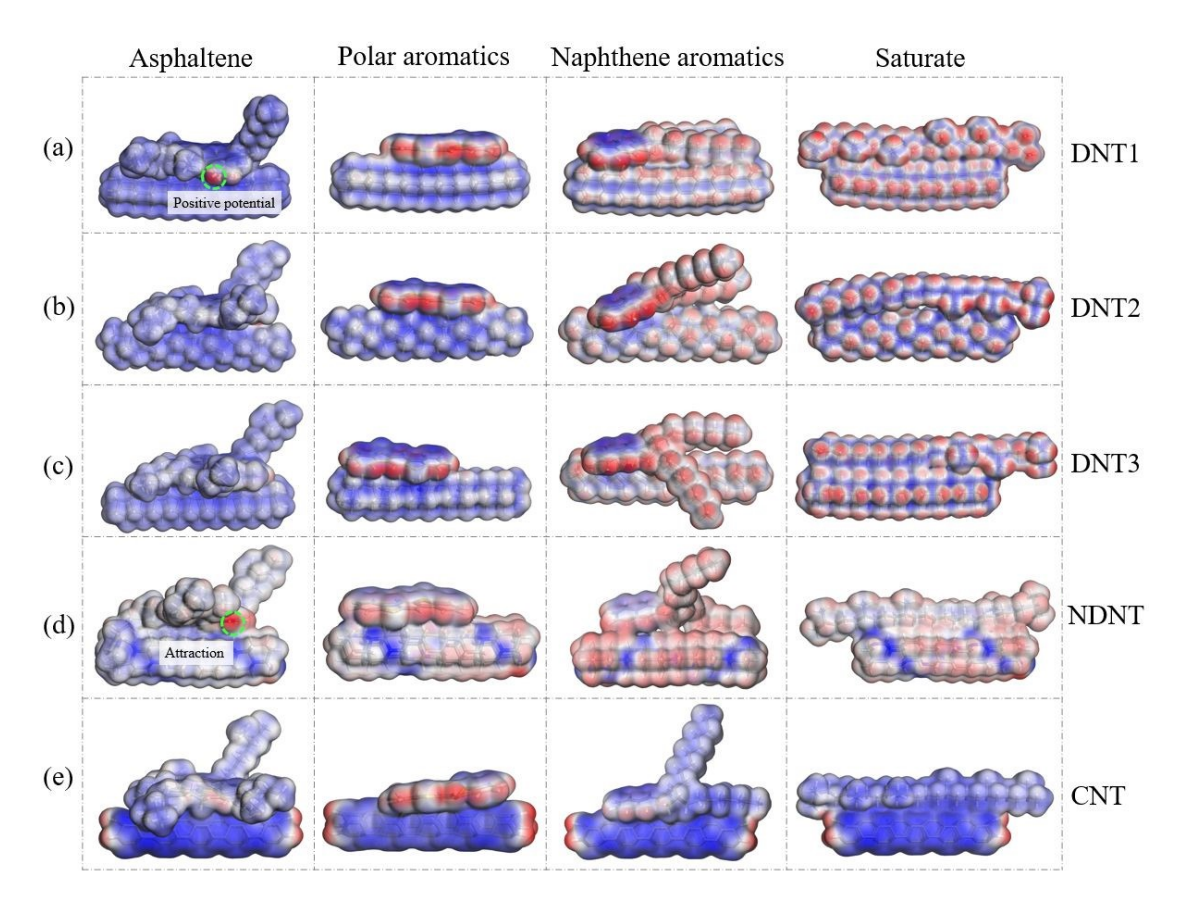


Figure 13 Molecular electrostatic potentials between asphalt components and (a) DNT1,

(b) DNT2, (c) DNT3, (d) NDNT, and (f) CNT through DFT calculation.

This article is licensed under a Creative Commons Attribution-NonCommercial 3.0 Unported Licence

Open Access Article. Published on 28 2025. Downloaded on 02.11.2025 20:14:45.

2

3

4

5

6

7

8

9

10

11

12

13

14

15

16

17

18

19

20

21

View Article Online DOI: 10.1039/D5NR03427B

4 Conclusion and discussion

4.1 Conclusion

The shear resistance and interfacial properties of asphalt nanocomposites reinforced with DNTs and CNTs are investigated through MD simulations, focusing on interfacial interactions during the pullout process. The findings reveal that NDNT modified asphalt nanocomposites exhibit the higher viscosity and T_{g} values compared to other DNTs, while CNT modified composites demonstrate the greater pullout force than those reinforced with DNTs. This improvement in shear resistance is primarily due to π - π stacking interactions that facilitate the wrapping of asphalt molecules around CNT surfaces. This improvement in shear resistance is crucial for pavement applications, as it enhances the material's ability to withstand mechanical stresses and reduce deformation over time. Among the DNTs, DNT2 modified asphalt nanocomposites show the highest pullout performance, attributed to DNT2's helical structure, which promotes the mechanical interlocking and reduces the relative movement within the asphalt matrix. Additionally, the hydrogenated surface of DNT enhances interactions with asphalt molecules, and the formation of O-H···N hydrogen bonds between hydroxyl groups on asphaltene-phenol and nitrogen atoms on NDNT While the binding energy between CNT and further increases the shear resistance. asphalt is slightly lower than that of NDNT, it remains significantly higher than that of DFT calculations indicate that nitrogen doping modifies the electronic DNTs.

1

2

3

4

5

6

7

8

9

10

11

12

13

14

15

16

17

18

19

20

21

structure of NDNT, resulting in localized negative charges that enhance electronegativity, while delocalized π -electrons in CNTs improve adhesion and load transfer capabilities. These findings suggest that incorporating NDNTs and CNTs into asphalt mixtures can lead to more sustainable and resilient pavement materials with Overall, this study underscores the considerable improved long-term durability. potential of DNTs, NDNTs, and CNTs in developing sustainable and resilient asphalt nanocomposites for the pavement industry. Importantly, our research extends beyond payement applications, offering broader implications for materials science and By clarifying the interfacial interactions and mechanisms at play, nanotechnology. our work paves the way for further exploration of nanomaterials in various composite systems, promoting interdisciplinary research and collaboration.

By investigating the shear resistance and interfacial properties of asphalt nanocomposites reinforced with DNTs and CNT through molecular dynamics simulations, we explore fundamental interactions that enhance the performance of The unique properties of DNTs, such as their helical structure and asphalt material. hydrogenated surfaces, significantly improve mechanical interlocking and interfacial interactions with asphalt, which are critical for developing sustainable and resilient Additionally, our findings on the electronic structure modifications due to nitrogen doping in NDNTs further contribute to understanding how nanomaterials can optimize the performance of composite systems. By examining these differences at the atomistic level, our study not only clarifies the unique roles of DNTs and CNTs but

View Article Online

also contributes new insights into optimizing asphalt nanocomposites for improved

durability and performance. This emphasis on comparative analysis and the exploration of new reinforcement mechanisms represents a significant advancement over prior works, paving the way for more effective applications of nanomaterials and other nanocomposite materials across various applications, including lightweight

structural materials, energy storage systems, and advanced coatings. Our work not

7 only addresses the immediate challenges in asphalt technology but also opens avenues

for interdisciplinary research that could benefit a wide range of applications.

4.2 Discussion

While MD simulations are effective for investigating the interfacial interactions of various materials, they inherently operate on a time scale ranging from nanoseconds to microseconds. This limitation restricts the ability to observe the long-term behaviors of asphalt nanocomposites, including aging and fatigue processes. Consequently, although we have revealed the improvements of DNT/CNT in shear resistance and interfacial properties, these enhancements may not accurately reflect the performance of asphalt materials over extended periods in real-world conditions. To address these limitations, future research could include complementary approaches, such as experimental studies that monitor the long-term performance of DNT/CNT modified asphalt nanocomposites under realistic conditions. Additionally, employing multiscale modeling techniques that bridge the gap between molecular dynamics and continuum mechanics could provide valuable insights into the macroscopic behavior of

these materials over longer time scales.

1

2

3

4

5

6

7

8

9

10

11

12

13

14

15

16

17

18

19

The effectiveness of nanomaterials in enhancing asphalt properties relies heavily on the interfacial interactions between the nanomaterials and the asphalt matrix. homogeneous distribution, each nanomaterial can interact uniformly with asphalt molecules, promoting effective load transfer and increased shear resistance. However, in a heterogeneous arrangement, some regions may experience stronger interactions while others may not benefit from the reinforcement, leading to inconsistent This variability in distribution can arise from factors such as mixing performance. techniques and processing conditions, which may not be fully controlled in practical applications. In the MD simulations, we assume a homogeneous distribution of nanomaterials within the asphalt matrix. Consequently, the mechanical properties of the asphalt nanocomposite between the simulations and experiments may exhibit discrepancies. Therefore, future studies should explore the effects of different nanomaterial distributions to provide a more comprehensive understanding of their impact on asphalt performance.

Acknowledgments

The authors are grateful for the support from National Natural Science Foundation of China (Grant No. 42277175 and No. 12102162), and Guizhou Provincial Major Scientific and Technological Program (2023-425).

20

21

This article is licensed under a Creative Commons Attribution-NonCommercial 3.0 Unported Licence

Open Access Article. Published on 28 2025. Downloaded on 02.11.2025 20:14:45.

View Article Online DOI: 10.1039/D5NR03427B

- T. Nian, P. Li, J. Ge, J. Song and M. Wang, Green environmental protection and 2
- sustainable utilization of straw: Investigation for molecular dynamics of highland 3
- barley straw fiber to enhancing road performance of asphalt, J Clean Prod, 2024, 452. 4
- A. Behnood, A review of the warm mix asphalt (WMA) technologies: Effects on 5
- thermo-mechanical and rheological properties, J Clean Prod, 2020, 259. 6
- 3. X. Luo, J. Xu and F. Ma, Thermodynamics of healing of asphalt binders with free 7
- energy, Mech. Mater., 2023, 185, 104757. 8
- 9 M. S. Bello, Y. Zhang, X. Wang and N. S. A. Yaro, Recycling polymeric healthcare
- 10 waste in asphalt pavements towards sustainable roads: A technical review, J Clean Prod,
- 11 2024, **480**, 144068.
- 5. Y. Wang, W. Wang and L. Wang, Understanding the relationships between 12
- 13 rheology and chemistry of asphalt binders: A review, Constr Build Mater, 2022, 329,
- 14 127161.
- C. Yan, J. Yan, Z. Zhang, D. Yu, S. Wang, X. Jiang, C. Ai and Z. Leng, Screw 15
- extrusion process used in the polymer modified asphalt field: A review, J Clean Prod, 16
- 2024, 448. 17
- 18 7. H. Li, S. Liu, F. Yang, S. He, H. Jing, X. Zou, Z. Li and Y. Sheng, Review of
- 19 utilization of bamboo fiber in asphalt modification: Insights into preparation,
- 20 performance, reinforcement, and challenges, J Clean Prod, 2024, 468, 143010.
- P. Lin, X. Liu, S. Ren, Y. Li, J. Xu and M. Li, Unraveling the influence of fibers 21

- on aging susceptibility and performance of high content polymer modified asphalt 1
- mixtures, Case Stud Constr Mater, 2023, 18, e02211. 2
- 9. I. R. Segundo, E. Freitas, V. T. F. C. Branco, S. Landi, M. F. Costa and J. O. 3
- Carneiro, Review and analysis of advances in functionalized, smart, and 4
- multifunctional asphalt mixtures, Renew Sust Energ Rev, 2021, 151, 111552. 5
- 10. J. Zhou, A. I. Chizhik, S. Chu and D. Jin, Single-particle spectroscopy for 6
- 7 functional nanomaterials, *Nature*, 2020, **579**, 41-50.
- 11. K. Debbarma, B. Debnath and P. P. Sarkar, A comprehensive review on the usage 8
- 9 of nanomaterials in asphalt mixes, Constr Build Mater, 2022, 361, 129634.
- 10 12. D. Mitra, S. Faisal Kabir, A. Ali, Y. Mehta and M. Elshaer, Evaluation of the
- 11 impact of nanomodification on Self-Healing behavior of asphalt binders, Constr Build
- 12 Mater, 2023, 405, 133358.

This article is licensed under a Creative Commons Attribution-NonCommercial 3.0 Unported Licence

Open Access Article. Published on 28 2025. Downloaded on 02.11.2025 20:14:45.

- 13 13. D. Zhang, Z. Huang, G. Yuan, Y. Zheng, G. Qian, Z. You and H. Zhang, Research
- 14 anti-aging mechanism of SBS-modified asphalt compounded with
- multidimensional nanomaterials based on atomic force microscopy, Constr Build Mater, 15
- 2022, 317, 125808. 16
- 14. Y. Li, L. Yang, X. Jiang, Y. Lu, C. Han, Y. Tang and N. Yang, Diamond 17
- 18 Nanostructures at Different Dimensions: Synthesis and Applications, Adv. Funct.
- 19 Mater., 2024, 34.
- 15. H. Zhan, G. Zhang, V. B. Tan and Y. Gu, The best features of diamond nanothread 20
- 21 for nanofibre applications, *Nat Commun*, 2017, **8**, 14863.

- 1 16. H. Zhan, G. Zhang, X. Zhuang, R. Timon and Y. Gu, Low interfacial thermal View Article Online
- 2 resistance between crossed ultra-thin carbon nanothreads, *Carbon*, 2020, **165**, 216-224.
- 3 17. K. Duan, J. Zhang, L. Li, Y. Hu, W. Zhu and X. Wang, Diamond nanothreads as
- 4 novel nanofillers for cross-linked epoxy nanocomposites, *Compos. Sci. Technol.*, 2019,
- 5 **174**, 84-93.
- 6 18. X. Q. Wang, C. L. Chow and D. Lau, Topology-controlled thermomechanical
- 7 properties of diamond nanothread enhanced polymeric materials, *Appl Mater Today*,
- 8 2023, **32**, 101822.
- 9 19. Y. Feng, H. Hao, H. Lu, C. L. Chow and D. Lau, Exploring the development and
- 10 applications of sustainable natural fiber composites: A review from a nanoscale
- 11 perspective, *Compos B Eng*, 2024, **276**, 111369.
- 12 20. X. Q. Wang, W. Jian, O. Buyukozturk, C. K. Y. Leung and D. Lau, Degradation
- of epoxy/glass interface in hygrothermal environment: An atomistic investigation,
- 14 Compos B Eng., 2021, **206**.
- 15 21. W. Cui, W. Huang, H. M. Z. Hassan, X. Cai and K. Wu, Study on the interfacial
- 16 contact behavior of carbon nanotubes and asphalt binders and adhesion energy of
- modified asphalt on aggregate surface by using molecular dynamics simulation, *Constr*
- 18 Build Mater, 2022, **316**, 125849.
- 19 22. W. M. Ji and L. W. Zhang, Diamond nanothread reinforced polymer composites:
- 20 Ultra-high glass transition temperature and low density, Compos. Sci. Technol., 2019,
- 21 **183**, 107789.

- 1 23. B. B. Yin, J. S. Huang, W. M. Ji and K. M. Liew, Exploring frictional performance
- 2 of diamond nanothread reinforced polymer composites from the atomistic simulation
- and density functional theory, *Carbon*, 2022, **200**, 10-20.
- 4 24. X. Liu, R. Yang, Z. Bie, F. Nie, Y. Fan, E. Oterkus and X. He, Enhanced interfacial
- 5 thermal transport in diamond nanothread reinforced polymer nanocomposites: insights
- from atomistic simulations and density functional theory, *Nanoscale*, 2025, **17**, 13419-
- 7 13433.
- 8 25. F. Nie, X. Su, M. Wang, X. Ma, K. Ou, J. Liu and H. Lin, Debonding of asphalt-
- 9 aggregate interface under coupled moisture and temperature conditions: An atomistic
- 10 study, Case Stud Constr Mater, 2025, 22, e04554.
- 11 26. F. Nie, Z. Bie and H. Lin, Investigating the advanced thermomechanical properties
- of coiled carbon nanotube modified asphalt, *Constr Build Mater*, 2024, 441, 137512.
- 13 27. B. Cui and H. Wang, Molecular modeling of asphalt-aggregate debonding potential
- under moisture environment and interface defect, Appl Surf Sci. 2022, 606.
- 15 28. X. Ma, X. Zhu, T. Wang, T. Si and J. Fan, Unveiling the importance of surface
- ionization on desalination and ion-sieving performance of graphene oxide membranes,
- 17 Sep. Purif. Technol., 2024, **341**, 126930.
- 18 29. S. Kumar, Investigating effect of CNT agglomeration in CNT/polymer
- 19 nanocomposites using multiscale finite element method, *Mech. Mater.*, 2023, **183**,
- 20 104706.
- 21 30. Q. L. Xiong, S. A. Meguid, Y. Wang and G. J. Weng, Molecular dynamics and

- atomistic based continuum studies of the interfacial behavior of nanoreinforced epoxy, View Article Online

 1 atomistic based continuum studies of the interfacial behavior of nanoreinforced epoxy,
- 2 *Mech. Mater.*, 2015, **85**, 38-46.
- 3 31. F. Nie, W. Jian, Z. Yu, C. L. Chow and D. Lau, Mesoscale modeling to study
- 4 isolated asphaltene agglomerates, *Constr Build Mater*, 2023, **379**, 131249.
- 5 32. J. Zhang, L. Sun, H. Zhan, Y. Nie, Y. Pang, C. Bian and C. Lü, Impact of diamond
- 6 nanothread on the viscosity of asphalt binder: Insights from atomistic simulations, J
- 7 *Clean Prod*, 2024, **434**, 139945.
- 8 33. Z. Luo, J. Guo, X. Liu, Y. Mu, M. Zhang, M. Zhang, C. Tian, J. Ou and J. Mi,
- 9 Preparation of ceramsite from lead-zinc tailings and coal gangue: Physical properties
- and solidification of heavy metals, *Constr Build Mater*, 2023, **368**, 130426.
- 11 34. L. Luo, Y. Liu, M. Oeser, A. García Hernandez and P. Liu, Unraveling the nano-
- cracking mechanism in aged asphalt binder with consideration of rejuvenation effects,
- Engineering Fracture Mechanics, 2023, 292, 109683.
- 14 35. Y. Gao, X. Liu, S. Ren, E. I. Assaf, P. Liu and Y. Zhang, Nanostructure and damage
- 15 characterisation of bitumen under a low cycle strain-controlled fatigue load based on
- molecular simulations and rheological measurements, Compos B Eng. 2024, 275,
- 17 111326.
- 18 36. L. W. Zhang, W. M. Ji and K. M. Liew, Mechanical properties of diamond
- 19 nanothread reinforced polymer composites, *Carbon*, 2018, **132**, 232-240.
- 20 37. S. P. Patil, P. Shendye and B. Markert, Molecular dynamics simulations of silica
- 21 aerogel nanocomposites reinforced by glass fibers, graphene sheets and carbon

View Article Online

- 1
- 2 107884.
- 38. B. Cui and H. Wang, Molecular interaction of Asphalt-Aggregate interface 3
- modified by silane coupling agents at dry and wet conditions, Appl Surf Sci, 2022, 572, 4
- 5 151365.
- 39. D. D. Li and M. L. Greenfield, Chemical compositions of improved model asphalt 6
- 7 systems for molecular simulations, Fuel, 2014, 115, 347-356.
- 40. O. C. Mullins, The modified Yen model, Energy Fuels, 2010, 24, 2179-2207. 8
- 9 41. M. P. Koopmans, J. W. De Leeuw, M. D. Lewan and J. S. Sinninghe Damste,
- 10 Impact of dia- and catagenesis on sulphur and oxygen sequestration of biomarkers as
- 11 revealed by artificial maturation of an immature sedimentary rock, Org. Geochem.,
- 12 1996, **25**, 391-426.
- 13 42. X. Lu, B. Kalman and P. Redelius, A new test method for determination of wax
- 14 content in crude oils, residues and bitumens, Fuel, 2008, 87, 1543-1551.
- 43. B. Cui, X. Gu, D. Hu and Q. Dong, A multiphysics evaluation of the rejuvenator 15
- effects on aged asphalt using molecular dynamics simulations, J Clean Prod, 2020, 16
- 17 259.
- 18 44. M. Olbrich, P. Mayer and D. Trauner, A step toward polytwistane: synthesis and
- 19 characterization of C₂-symmetric tritwistane, Org. Biomol. Chem., 2014, 12, 108-112.
- 45. X. Li, T. Wang, P. Duan, M. Baldini, H.-T. Huang, B. Chen, S. J. Juhl, D. 20
- Koeplinger, V. H. Crespi, K. Schmidt-Rohr, R. Hoffmann, N. Alem, M. Guthrie, X. 21

- 1 Zhang and J. V. Badding, Carbon Nitride Nanothread Crystals Derived from Pyridine, View Article Online

 View Article Online

 View Article Online

 View Article Online
- 2 J. Am. Chem. Soc., 2018, **140**, 4969-4972.
- 3 46. S. Liu, H. Wang, J. Yang, S. Luo, Y. Liu, W. Huang, J. Hu, G. Xu and Z. Min,
- 4 Force field benchmark of asphalt materials: Density, viscosity, glass transition
- 5 temperature, diffusion coefficient, cohesive energy density and molecular structures, J.
- 6 *Mol. Liq.*, 2024, **398**, 124166.
- 7 47. H. Zhang, J. Cao, H. Duan, H. Luo and X. Liu, Molecular dynamics insight into
- 8 the adsorption and distribution of bitumen subfractions on Na-montmorillonite surface,
- 9 Fuel, 2022, **310**.
- 10 48. M. Zhang, Y. Yu, Y. Luan, H. Zhou, X. Peng, L. Gong and H. Zhou, Effects of
- 11 CNT microstructural characteristics on the interfacial enhancement mechanism of
- carbon fiber reinforced epoxy composites via molecular dynamics simulations, *Thin-*
- 13 *Walled Struct* 2024, **195**.
- 14 49. Y. Pang, L. Sun, H. Zhan, X. Zheng, J. Zhang, C. Bian and C. Lü, Assessing the
- 15 impact of ultra-thin diamond nanothreads on the glass transition temperature of a
- 16 bituminous binder, *Nanoscale Adv*, 2023, **5**, 6724-6735.
- 17 50. W. Jian, D. Hui and D. Lau, Nanoengineering in biomedicine: Current
- development and future perspectives, 2020, 9, 700-715.
- 19 51. B. Hess, Determining the shear viscosity of model liquids from molecular
- 20 dynamics simulations, *J. Chem. Phys.*, 2002, **116**, 209-217.
- 21 52. F. Khabaz and R. Khare, Glass transition and molecular mobility in Styrene-

- Butadiene rubber modified asphalt, *J Phys Chem B*, 2015, **119**, 14261-14269. DOI: 10.1039/D5NR03427B 1
- 53. L. Luo, A. M. Awed, M. Oeser and P. Liu, Mechanisms of interfacial load transfer 2
- in the fracture process of carbon nanotube-reinforced bitumen composites, Eng. Fract. 3
- Mech., 2023, 290. 4
- 54. M. Bursch, J. M. Mewes, A. Hansen and S. Grimme, Best-Practice DFT Protocols 5
- for Basic Molecular Computational Chemistry, Angew. Chem. Int. Ed. Engl., 2022, 61, 6
- e202205735. 7
- 55. J. Ge, H. Yu, G. Qian, W. Dai, C. Zhang, C. Shi, H. Zhou, T. Nian and Y. Zhong, 8
- 9 Enhancement mechanism of aggregate surface roughness structure on interfacial
- 10 properties of asphalt mixtures, Constr Build Mater, 2024, 449, 138388.
- 56. G. Xu and H. Wang, Molecular dynamics study of oxidative aging effect on asphalt 11
- 12 binder properties, *Fuel*, 2017, **188**, 1-10.
- 13 57. L. Zhang and M. L. Greenfield, Rotational relaxation times of individual
- 14 compounds within simulations of molecular asphalt models, The Journal of Chemical
- Physics, 2010, 132. 15
- 58. Y. Huang, Z. Wu, L. Liang, J. Ying, L. Gui, P. Kang Shen and Z. Q. Tian, 16
- Revealing the dependance of mechanical properties of asphalt binder on graphene size 17
- 18 via multi-scale methods, *Mater Des*, 2023, **236**, 112478.

View Article Online

DOI: 10.1039/D5NR03427E

Data availability

The raw simulation data, input files for the LAMMPS simulations ¹, and analysis scripts used to generate the findings reported in this study are not publicly deposited in a repository due to their large size and specialized formatting, but are available from the corresponding author, Dr. Xuefeng LIU (xfliu6-c@my.cityu.edu.hk), upon reasonable request. The CVFF force field parameters used in this study are derived from previously published and cited works ^{2, 3}, while the LAMMPS software package ⁴ employed for the simulations is publicly available. Additionally, all other relevant data and methodological details necessary for understanding and reproducing the conclusions of this manuscript are provided within the article.

Reference

- A. P. Thompson, H. M. Aktulga, R. Berger, D. S. Bolintineanu, W. M. Brown, P. S. Crozier, P. J. in 't Veld, A. Kohlmeyer, S. G. Moore, T. D. Nguyen, R. Shan, M. J. Stevens, J. Tranchida, C. Trott and S. J. Plimpton, LAMMPS - a flexible simulation tool for particle-based materials modeling at the atomic, meso, and continuum scales, *Comput. Phys. Commun.*, 2022, 271, 108171.
- 2. F. Nie, W. Jian and D. Lau, An atomistic study on the thermomechanical properties of graphene and functionalized graphene sheets modified asphalt, *Carbon*, 2021, **182**, 615-627.
- 3. P. Dauber-Osguthorpe, V. A. Roberts, D. J. Osguthorpe, J. Wolff, M. Genest and A. T. Hagler, Structure and energetics of ligand binding to proteins: Escherichia coli, dihydrofolate reductasetrimethoprim, a drug-receptor system, *Proteins*, 1988, 4, 31-47.
- 4. S. Plimpton, Fast Parallel Algorithms for Short-Range Molecular Dynamics, *Journal of Computational Physics*, 1995, **117**, 1-19.